

PART II: FUEL OXIDATION KINETICS MODEL FOR OPERATING DEFECTIVE FUEL ELEMENTS

B.J. Lewis, W.T. Thompson, F. Akbari, C. Thurgood and J. Higgs
 Department of Chemistry and Chemical Engineering
 Royal Military College of Canada
 PO Box 17000, Kingston, Ontario K7K 7B4

ABSTRACT

A theoretical treatment has been developed to predict the fuel oxidation behaviour in operating defective nuclear fuel elements. The equilibrium stoichiometry deviation in the hyperstoichiometric fuel has been derived from thermodynamic considerations. The kinetics model accounts for multi-phase transport including interstitial oxygen diffusion in the solid and gas-phase transport of hydrogen and steam in the fuel cracks. The fuel oxidation model is further coupled to a heat conduction model to account for the feedback effect of a reduced thermal conductivity in the hyperstoichiometric fuel. A numerical solution has been developed using a finite element technique with the FEMLAB software package.

The model has been compared to available data from several in-reactor X-2 loop experiments with defective fuel conducted at the Chalk River Laboratories. The model has also been benchmarked against an O/U profile measurement for a spent defective fuel element discharged from a commercial reactor.

1. INTRODUCTION

With defective fuel, a primary leak path exists so that coolant can enter into the fuel element, permitting oxidation of both the fuel and cladding. The fuel oxidation process itself can affect the thermal performance of the element. In response to this issue, a mechanistic model has been developed to predict fuel oxidation behaviour in operating defective fuel elements.

2. MODEL DEVELOPMENT

During in-reactor operation, a temperature gradient develops due to internal fission heating. Steam present in the fuel-to-clad gap of a defective fuel rod can penetrate through cracks in the pellet by gas phase transport and react with the fuel resulting in an oxygen profile in the pellet since the thermodynamics of the oxidation reaction is temperature dependent. A re-distribution of the interstitial oxygen ions can also occur due to solid-state diffusion. Any hydrogen generated from both the Zircaloy clad and fuel oxidation processes will also affect the oxygen potential in the gaseous atmosphere.

The transport delivery mechanism is therefore a complicated problem where gas and solid-state radial diffusion equations must be coupled by a kinetically-limited reaction law at the crack surfaces (see Fig. 1). In particular, the H₂O/H₂ gas mixture in the gap will diffuse radially through a network of cracks where a reaction occurs with the solid fuel. The reaction products, consisting of H₂ in the gas in the cracks and interstitial oxygen ions in the solid fuel, are then transported via diffusion in their respective phase (Fig. 1). Due to the lower fuel surface temperature, the outer pellet surface will remain essentially stoichiometric.

The rate of reaction of UO_{2+x} with a gas mixture containing steam and hydrogen at partial pressures of $p_{H_2O} = (1-q) p_t$ and $p_{H_2} = q p_t$ is given by:¹

$$R_{ox} = c_U \alpha \sqrt{(1-q)p_t} (x_e - x(t)) \quad (1)$$

where R_{ox} is the reaction rate in moles O (or H₂) m⁻² s⁻¹, $c_U = 4.1 \times 10^4$ mol m⁻³ is the molar density of uranium in UO₂, $\alpha = 0.365 \exp(-23500/T)$ (in m s⁻¹) is the surface exchange coefficient at temperature T (in K), q is the mole fraction of H₂ in the cracks and $p_t = 100$ atm is the total system pressure. The equilibrium oxidation state of the fuel x_e can be obtained by equating the oxygen potential in the local atmosphere with the oxygen potential in the solid fuel. The oxygen partial pressure p_{O_2} (atm) in the atmosphere can be obtained from a solution of the cubic equation:¹

$$4(p_{O_2})^3 + 4[(p_{H_2})_i - K_2^*]p_{O_2}^2 + [(p_{H_2})_i^2 + 4(p_{H_2O})_i K_2^*]p_{O_2} - (p_{H_2O})_i^2 K_2^* = 0 \quad (2)$$

where $(p_{H_2O})_i$ and $(p_{H_2})_i$ are the initial steam and hydrogen partial pressure quantities and the equilibrium constant K_2^* for water dissociation is given by:²

$$\log K_2^* = -\frac{25032}{T} + 1.9588 \log T - 0.96630 \quad (3)$$

The solution of Eq. (2) can be equated to the oxygen partial pressure in the fuel using the Blackburn thermochemical model:³

$$\ln p_{O_2} = 2 \ln \left(\frac{x_e(2+x_e)}{1-x_e} \right) + 108x_e^2 - \frac{32700}{T} + 9.92 \quad (4)$$

Thus, x_e can then be solved for in Eq. (4). As shown in Part I, the Blackburn model is in good agreement with an extensive thermodynamic analysis performed with the Facility for Analysis of Chemical Thermodynamics (FACT).⁴

With the fuel oxidation reaction, $UO_2 + xH_2O \rightarrow UO_{2+x} + xH_2$, the transport equation for O diffusion in the fuel pellet is given by:

$$c_U \frac{\partial x}{\partial t} = c_U \bar{\nabla} \cdot (D \bar{\nabla} x) + \sigma R_{ox} \quad (5)$$

where σ is the surface area of cracks per unit volume of fuel (m⁻¹) for the cracked fuel body. Here D is taken as the chemical diffusion coefficient for oxygen:⁵

$$D = 2.5 \times 10^{-4} \exp\left(-\frac{16400}{T}\right) \text{ m}^2 \text{ s}^{-1} \quad (6)$$

The diffusion coefficient in Eq. (5) cannot be assumed to be independent of position because of the strong temperature dependence. Thus, assuming only radial diffusion in a cylindrical fuel pellet of radius a , Eq. (5) becomes:

$$\frac{\partial x}{\partial t} = \sigma \alpha \sqrt{(1-q)p_t} \{x_e - x(t)\} + \frac{1}{r} \left[\frac{\partial}{\partial r} \left(D r \frac{\partial x}{\partial r} \right) \right] \quad (7)$$

The fuel pellet is initially assumed to be stoichiometric:

$$x = 0, \quad 0 \leq r \leq a, \quad t = 0. \quad (8a)$$

Symmetry is considered with the use of a reflexive boundary condition at the centre of the pellet:

$$\frac{\partial x}{\partial r} = 0, \quad r = 0, \quad t > 0. \quad (8b)$$

At the surface of the pellet, where the temperature is lower, the fuel essentially remains stoichiometric so that:

$$x \approx 0, \quad r = a, \quad t > 0. \quad (8c)$$

In previous work, the hydrogen-to-steam ratio was fixed and assumed to remain constant throughout the pellet.¹ However, in this analysis, the impact of hydrogen generation from the fuel oxidation process is modelled by including a diffusion equation for the hydrogen mole fraction q in the cracked fuel body (see Fig. 1). The cracked solid is assumed to have a porosity ε , defined as the ratio of the volume of cracks (and/or pores) to that of the solid fuel i.e., V_{cracks}/V_{fuel} . Thus, as follows from the mass balance, the hydrogen molar concentration ($c_g q$) in the cracks is given by:⁶

$$\varepsilon \frac{\partial(c_g q)}{\partial t} = \varepsilon \bar{\nabla} \cdot (c_g D_g \bar{\nabla} q) + \sigma R_{ox} \quad (9)$$

where c_g is the total molar concentration of gas (mol m^{-3}) (assumed to be ideal) ($= p/RT$ and $R = 82.057 \times 10^{-6} \text{ m}^3 \text{ atm mol}^{-1} \text{ K}^{-1}$ is the ideal gas constant). Equivalently, for radial diffusion with a tortuosity factor τ for the diffusion path in the cracked solid, Eq. (9) becomes:

$$\varepsilon c_g \frac{\partial q}{\partial t} = c_U \sigma \alpha \sqrt{(1-q)p_t} \{x_e - x(t)\} + \frac{\varepsilon}{\tau^2 r} \left[\frac{\partial}{\partial r} \left(c_g D_g r \frac{\partial q}{\partial r} \right) \right] \quad (10)$$

In the development of Eq. (10), a quasi-static assumption has been used for the total molar concentration.⁶ The quantity $c_g D_g$ (in $\text{mol m}^{-1} \text{ s}^{-1}$) is evaluated from the Chapman-Enskog kinetic theory for gases:⁷

$$c D_g = 2.2646 \times 10^{-3} \sqrt{T \left(\frac{1}{M_{H_2}} + \frac{1}{M_{H_2O}} \right)} \sigma_{AB}^2 \Omega_{AB} \quad (11)$$

where T is the temperature (K), M is the molecular weight (in g mol^{-1}), σ_{AB} (\AA) is the combined collision diameter and Ω_{AB} is the collision integral. The combined parameters are evaluated from individual Lennard-Jones force constants for H_2 and H_2O .^{7,8}

Equation (10) is subject to the initial condition:

$$q = q_1, \quad 0 \leq r \leq a, \quad t = 0, \quad (12a)$$

where q_1 is taken as an initial hydrogen mole fraction in the fuel-to-clad gap. Symmetry at the centre of the pellet is again considered with the use of a reflexive boundary condition:

$$\frac{\partial q}{\partial r} = 0, \quad r = 0, \quad t > 0. \quad (12b)$$

At the surface of the pellet, hydrogen is present in the fuel-to-clad gap due, for instance, to the Zircaloy oxidation process. Thus, in the current analysis, it is assumed that the hydrogen mole fraction is again equal to a constant value of q_1 :

$$q = q_1, \quad r = a, \quad t > 0. \quad (12c)$$

For a solution of these transport equations, the temperature profile must also be known, which can be obtained from the (steady-state) heat conduction equation⁹

$$\rho C_p \frac{\partial T}{\partial t} = \frac{1}{r} \frac{\partial}{\partial r} \left(rk \frac{\partial T}{\partial r} \right) + \frac{P}{\pi a^2} \left[\frac{(\kappa a)}{2I_1(\kappa a)} \right] I_0(\kappa r) = 0 \quad (13)$$

where k is the thermal conductivity, ρ is the density and C_p is the specific heat for the solid, P is the linear power of the fuel rod and κ is the inverse neutron diffusion length (e.g., $\kappa = 1.1 \text{ cm}^{-1}$ for naturally-enriched fuel at 8000 MWd/t). Equation (13) is further coupled to the other two partial differential equations because the thermal conductivity is also a function of x . The thermal conductivity model is taken from Ref. 1 and employs the Ellis, Porter and Shaw model for the phonon contribution.¹⁰ Similarly, Eq. (13) is subject to the conditions:

$$\frac{\partial T}{\partial r} = 0, \quad r = 0, \quad t > 0 \quad (14a)$$

and

$$T = T_1, \quad r = a, \quad t > 0 \quad (14b)$$

where T_1 is the fuel surface temperature. A steady-state heat conduction equation is considered in the current treatment since a steady-state temperature distribution is quickly approached under normal operating conditions. To account for the effects of a reduced heat transfer in the fuel-to-sheath gap and pellet expansion due to thermal effects, the fuel surface temperature T_1 was estimated from a previous simulation of the X-2 defect fuel experiments with the ELESIM fuel performance code.^{11,12}

3. RESULTS

The system of partial differential equations in Section 2 are solved numerically using a finite element method with the commercial FEMLAB software package (Version 2.3).¹³ The simulations are compared to gravimetric data of the average O/U ratio derived from in-reactor loop experiments with defective fuel rods at the Chalk River Laboratories (CRL) (Sections 3.1) and with oxygen profile data for a commercial spent defective rod (Section 3.2).

3.1 Simulation of CRL Defect Experiments

The defect experiments FDO-687, FFO-103, FFO-102-2 and FFO-104 from Ref. 11 have been considered in the current analysis since measured O/U data are available or it is suggested that fuel centreline melting has perhaps been observed in the ceramographic examinations. The model input for these experiments are detailed in Table 1. A comparison of the simulation results with experimental observations is also summarized in Table 1. The predicted profiles of the hydrogen mole fractions, stoichiometry deviations and fuel temperatures are shown in Figs. 2(a) to (d).

For the current analysis, ε is estimated from $1 - \rho/\rho_{TD}$, where ρ is the density of the UO_2 fuel ($\sim 10.7 \text{ g cm}^{-3}$) and ρ_{TD} is the theoretical density of the fuel ($= 10.96 \text{ g cm}^{-3}$). From the results of out-of-pile experiments, the crack surface area-to-fuel volume σ was taken as three times the geometric surface-to-volume ratio of the fuel (i.e., $\sigma = 1350 \text{ m}^{-1}$).¹⁴ This parameter determines how quickly the equilibrium stoichiometry deviation is reached; however, the model is not overly sensitive to this quantity since

equilibrium was quickly reached (see Fig. 3). The tortuosity τ was obtained by fitting the model to the experimental results of FFO-103, where it was assumed that pure steam is present in the fuel-to-clad gap for the multi-slit rod, i.e., $q_1 \sim 0$. The fuel surface temperature T_1 was set at 870 K based on the ELESIM results. The parameter τ was therefore adjusted until a maximum value of the (pellet-average) stoichiometry deviation was reached. This procedure yielded a value of $\tau \sim 1.023$ and pellet average O/U ratio of 2.17 (compared to a measured ratio of 2.28). As such, the model was able to predict the suggested fuel centreline melting seen in FFO-103 (Table 1), with a maximum fuel temperature of 2860 K at a fuel linear rating of ~ 50 kW/m. Fuel melting occurs at this temperature due to a reduced solidus and liquidus temperature in the hyperstoichiometric fuel as illustrated in the phase diagram in Part I (see also Fig. 4).⁴

For the other simulations, the previously derived value of τ was used. Since the fuel surface temperature T_1 did not change significantly with linear power in the ELESIM analysis (i.e., typically within ~ 150 K), this parameter was also conservatively kept constant at 870 K for the other experiments. Thus, the only adjustable parameter in the model is the hydrogen mole fraction in the fuel-to-clad gap, q_1 (which depends on the defect characteristics). Hence, for experiments FFO-102-2 and FFO-104, the value of q_1 was adjusted to match the post-test measured stoichiometry deviations (Table 1). Melting was subsequently predicted for the very high-powered element in FFO-102-2, whereas no melting was predicted for FFO-104 as supported by the ceramographic examination. For FDO-687, the value of q_1 was also adjusted to match the suggested experimental observation of fuel centreline melting at 64 kW/m in Phase I for element RPR. Interestingly, using this fixed value of q_1 , no melting is predicted to occur at 55 kW/m for the other elements in this experiment as also observed.¹⁵ Consequently, no fuel melting would be expected for drilled elements as well at an even lower power of 48 kW/m, as demonstrated in the previous experiment FDO-681. In addition, if fuel oxidation effects are ignored, no melting is further predicted with the model for the fuel rods RPL and RPP (which were used in FDO-681) that had operated intact at higher powers from 60 to 75 kW/m in an earlier irradiation.

In summary, the model is able to reasonably match the available O/U measurements and observed melting behaviour (Table 1). This behaviour is related to the defect size and the amount of steam available in the fuel-to-clad gap, i.e., the atmospheric oxygen potential of the gas mixture. For instance, in the multi-slit test of FFO-103 where there is unrestricted coolant entry such that $q_1 = 0$, melting occurs at a relatively lower power of ~ 50 kW/m. On the other hand, for the other artificially (FDO-687) and naturally (FFO-102-2) defected elements, the defect sizes were more restricted so that some hydrogen is available in the gap (i.e., due to clad and fuel oxidation processes), where q_1 is typically of the order of $\sim 0.1\%$. As such, melting does not occur at this same linear rating of 48 kW/m in the drilled elements of FDO-681. On the other hand, in FFO-104, with small hydride cracks where coolant entry appeared to be more restricted (as evidenced by a relatively low measured O/U ratio of 2.026 and a higher suggested H_2 mole fraction of $q_1 \sim 40\%$), no melting was observed or predicted at 58 kW/m.

3.2 Simulation of a Spent Commercial Defective Element

Similarly, the post-defect irradiation of a fuel element from a commercial CANDU reactor has been simulated with the FEMLAB model (Fig. 5(a)). The simulation can be compared to a measured O/U profile as determined by a coulometric titration method and with ceramography performed during a post-irradiation examination at the CRL (Fig. 5(b)).¹⁶

Unfortunately, the post-defect residence time was not clearly established for this element, where it was speculated that the element had remained in the defect state for greater than ~ 10 d. In addition, the irradiation was not typical, where after a period of operation from 23-29 kW/m, the bundle was shifted to an outer channel position where it remained for 40 d at a very low power of ~ 2 kW/m.¹⁷ Thus, in the

simulation, the rod was assumed to operate at 29 kW/m for ~15 d, after which the model was re-started (i.e., with the profile obtained from the end of the 15-d simulation) for a remaining irradiation at 2 kW/m for 40 d. For this lower-powered element, the fuel surface temperature was taken as ~800 K during the first irradiation at 29 kW/m and ~600 K during the second operating period at 2 kW/m. The same fixed values of the model parameters of τ , ε and σ as in Section 3.1 were assumed (Table 1).

The value of q_1 was again adjusted to reproduce the averaged measured O/U ratio of 2.044 (Table 1). Due to the low temperatures experienced during the second period of operation at 2 kW/m, no significant diffusion occurred so that the stoichiometry deviation profile did not change from that which had occurred in the previous higher-power period. Interestingly, the fitted value of q_1 (i.e., ~0.2%) is close to that obtained for the drilled (FDO-687) and naturally (FFO-102-2) defected elements, where some fuel exposure had also occurred (Table 1).

In Fig. 5(b) it can be seen that the measured O/U profile (i.e., near the secondary defect site) is more peaked than that which is predicted by the model. The model indicates that the stoichiometry deviation profile should flatten out during irradiation as a result of interstitial oxygen diffusion via the chemical diffusion coefficient. A more peaked profile is predicted with the model when solid-state diffusional effects are ignored or the diffusion coefficient is reduced (i.e., when an oxygen self-diffusion coefficient is employed).

4. DISCUSSION

The discrepancy in the O/U profile shown in Fig. 5 may perhaps be explained by post-shutdown operations. For instance, it is conceivable that some of the observed oxidation in the post irradiation examination (i.e., higher oxide states) could have been produced after reactor shutdown perhaps during long-term fuel storage in pools (which contain dissolved oxygen), as well as from fuel transfer and shipping operations (where moist air may be present).⁶

In particular, at lower temperatures (i.e., less than ~ 400°C), the presence of oxygen, with the presence of perhaps moisture and gamma radiation, may lead to formation of the higher oxides U_4O_9 , U_3O_7 and U_3O_8 .¹⁸⁻²² At lower temperatures, the possibility for solid-state diffusion of oxygen into the solid is significantly reduced. Hence, if defective fuel were exposed to moist air or to water containing dissolved air during post-shutdown operations, the kinetic reactions would be relatively slow (at the lower temperatures) and therefore one would only expect to see localized oxidation with the presence of perhaps higher oxides on exposed fuel surfaces. Interestingly, in the recent ceramography of the defective fuel rod, higher oxide states were seen locally, typically on exposed surfaces at pellet interface positions and along radial cracks.²³ Moreover, higher oxide states do not occur at higher temperatures during in-reactor operation due to thermodynamic constraints (especially in the presence of hydrogen generated during fuel and cladding oxidation). If the O/U ratios that are measured in the post-irradiation examination are higher than that which had actually occurred during in-reactor operation, a fitting of the model to these measured results would result in conservative predictions of the fuel temperatures as well as a possible overprediction of the extent of fuel centreline melting.

The current model requires *a priori* the H_2 mole fraction q_1 in the gas mixture of the gap as a boundary condition. This quantity can be achieved more fundamentally by coupling the given fuel oxidation equations to a gap transport model which accounts for steam penetration through the defect site(s), in order to determine the axial distribution of the oxygen potential in the fuel-to-clad gap.²⁴

Finally, the surface-exchange coefficient α in Eq. (1) is only strictly applicable to oxidizing conditions. However, during fuel reduction (i.e., with the presence of hydrogen gas), the stoichiometry kinetics are observed to be much more rapid as the physical process for removal of oxygen are different.²⁵ This enhanced process may result from either diffusion through the solid fuel, chemical reaction with hydrogen at the fuel surface or by mass transport through the boundary layer. Hence, neglecting the more rapid kinetics that result during fuel reduction should yield a more conservative estimate of the fuel oxidation state in the current analysis.

5. CONCLUSIONS

A model has been developed to account for the fuel oxidation kinetics in operating defective fuel rods. This treatment considers interstitial oxygen diffusion in the solid. In addition, hydrogen generated as a result of the fuel oxidation process and its gas-phase transport in the fuel cracks is further considered to determine the local oxygen potential throughout the cracked solid. The fuel oxidation model is also coupled to a heat conduction model. This mechanistic coupling enables a calculation of the temperature profile with fission heating, in which there is a feedback effect due to a degraded thermal conductivity in the hyperstoichiometric fuel. The physically-based equations of the model have been solved using a finite-element technique with the FEMLAB commercial software package.

The model has been used to interpret the thermal performance of defective fuel. In particular, the model has been fit to available data from several in-reactor loop experiments with defective fuel. The model has provided an estimate of the hydrogen-to-steam partial pressure ratio in the gap that is required to reproduce the (pellet-average) oxygen-to-uranium (O/U) ratio measured by gravimetric analysis. The defect characteristics will dictate the hydrogen-to-steam ratio in the fuel-to-clad gap that, in turn, will directly influence the local atmospheric oxygen potential and fuel thermal performance. Higher-powered defective fuel elements will reach a steady-state oxidation state in about a day of in-reactor operation. The model has been further benchmarked against an O/U profile measurement (i.e., using a coulometric titration method) of a defective fuel element discharged from a commercial reactor. It is not clear, however, if the measured profile is affected by post-shutdown operations (such as fuel transfer in air or long-term pool storage in pools containing dissolved oxygen).

6. ACKNOWLEDGEMENTS

The authors would like to acknowledge helpful discussions with Drs. R.A. Verrall and Z. He (CRL) on experimental O/U profile determination and ceramography examination. This work was sponsored by the CANDU Owners Group (COG) under work package WP 22324, the Natural Sciences and Engineering Research Council (NSERC) of Canada and the Director General of Nuclear Safety.

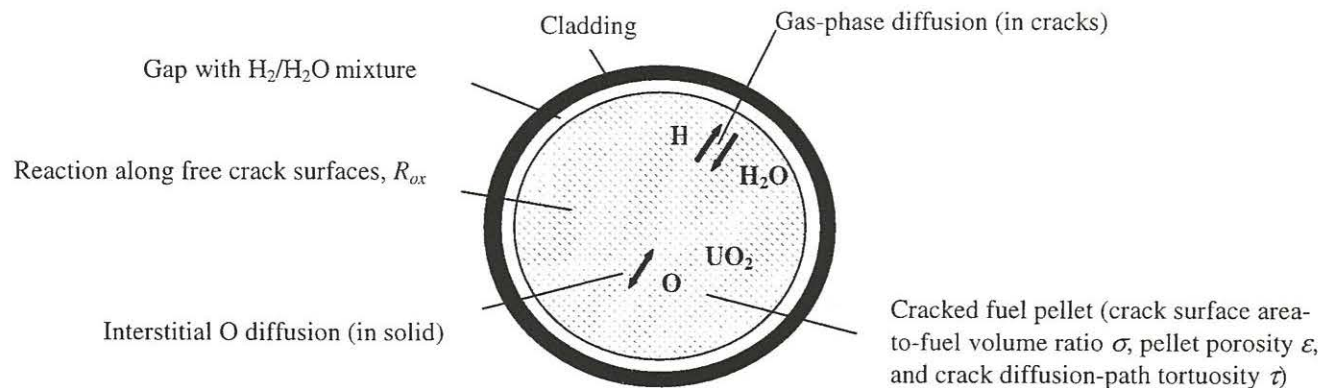
7. REFERENCES

1. B.J. Lewis, B. Szpunar and F.C. Iglesias, "Fuel Oxidation and Thermal Conductivity Model for Operating Defective Fuel Rods," *J. Nucl. Mater.* 306 (2002) 30.
2. O. Kubaschewski and C.B. Alcock, *Metallurgical Thermochemistry*, 5th ed., Pergamon, New York, 1979.
3. P.E. Blackburn, "Oxygen Partial Pressures over Fast Breeder Reactor Fuel, (I) A Model for UO_{2+x} ," *J. Nucl. Mater.* 46 (1973) 244.
4. W.T. Thompson, B.J. Lewis, F. Akbari And D.M. Thompson, "Part I: Thermodynamics Of Uranium Oxidation In Support Of Kinetics Model For Operating Defective Fuel Elements," 8th Int. Conf. on CANDU Fuel, Honey Harbour, Ontario, Sept. 21-24, 2003.
5. J.A. Meachen, "Oxygen Diffusion in Uranium Dioxide," *Nuclear Energy*, 28, No. 4, 221-226, 1989.
6. D.R. Olander, Y.S. Kim, W. Wang and S.K. Yagnik, "Steam Oxidation of Fuel in Defective LWR Rods," *J. Nucl. Mater.* 270 (1999) 11.
7. R.B. Bird, W.E. Stewart and E.N. Lightfoot, "Transport Phenomena," Wiley, New York, 1960.
8. R.C. Reid, J.M. Prausnitz and B.E. Poling, "The Properties of Gases and Liquids," McGraw-Hill Book Company, New York, 1987.
9. D.R. Olander, "Fundamental Aspects of Nuclear Reactor Fuel Elements," TID-26711-p1, U.S. Department of Energy (1976).
10. W.E. Ellis, J.D. Porter and T.L. Shaw, "The Effect of Oxidation, Burnup and Poisoning on the Thermal Conductivity of UO_2 : A Comparison of Data with Theory," Proc. International Topical Meeting on Light Water Reactor Fuel Performance, Park City, Utah, April 10-13, 2000, p. 715.
11. B.J. Lewis, R.D. MacDonald, N.V. Ivanoff and F.C. Iglesias, "Fuel Performance and Fission Product Release Studies for Defected Fuel Elements," *Nucl. Technol.* 103 (1993) 220.
12. B.J. Lewis, F.C. Iglesias, D.S. Cox and E. Gheorghiu, "A Model for Fission Gas Release and Fuel Oxidation Behaviour for Defected UO_2 Fuel Elements," *Nucl. Technol.* 92 (1990) 353-362.
13. "FEMLAB User's Guide and Introduction," COMSOL Inc., Burlington, MA, USA, 2001.
14. B.J. Lewis, B. Andre, B. Morel, P. Dehaut, D. Maro, P.L. Purdy, D.S. Cox, F.C. Iglesias, M.F. Osborne and R.A. Lorenz, "Modelling the Release Behaviour of Cesium During Severe Fuel Degradation," *J. Nucl. Mater.* 227 (1995) 83-109.
15. R.D. MacDonald, J.J. Lipsett, E.E. Perez and P.K. Kos, "Purposely Defected UO_2 -Zircaloy Fuel Elements Irradiated in Pressurized Light Water at Linear Powers of 55 kW/m," Atomic Energy of Canada Limited report, AECL-7751, May 1983.
16. R.A. Verrall, "Update on O/M Ratio Measurements in Defected Fuel and Error Estimation," Workshop on Fission Product Diffusion and Fuel Oxidation, Chalk River Laboratories, Chalk River, Ontario, August 26-29, 2002.
17. E. Kohn and M. Notley, private communication, 2002.
18. P. Taylor, D.D. Wood and D.G. Owen, "Crystallization of U_3O_8 and Hydrated UO_3 on UO_2 Fuel in Aerated Water Near 200°C," *J. Nucl. Mater.* 183 (1991) 105.
19. P. Taylor, R.J. Lemire and D.D. Wood, "The Influence of Moisture on Air Oxidation of UO_2 : Calculations and Observations," *Nucl. Technol.* 104 (1993) 164.
20. S. Sunder and N.H. Miller, "Oxidation of CANDU Uranium Oxide Fuel by Air in Gamma Radiation at 150°C," *J. Nucl. Mater.* 231 (1996) 121.
21. R.J. McEachern, "A Review of Kinetic Data on the Rate of U_3O_7 Formation on UO_2 ," *J. Nucl. Mater.* 245 (1997) 238.
22. R.J. McEachern and P. Taylor, "A Review of Oxidation of Uranium Dioxide at Temperatures Below 400°C," *J. Nucl. Mater.* 254 (1998) 87.
23. Z. He, "Ceramography of Defected Fuels," Workshop on Fission Product Diffusion and Fuel Oxidation, Chalk River Laboratories, Chalk River, Ontario, August 26-29, 2002.
24. B.J. Lewis, "An Overview of Defective Fuel Analysis in CANDU and Light Water Reactors," 6th Int. Conf. on CANDU Fuel, ISBN 0-919784-62-3, Niagara Falls, Ontario, Vol. 1, Sept. 26-29, 1999, pp. 403-427.
25. J. Abrefah, A. de Aguiar Braid, W. Wang, Y. Khalil and D.R. Olander, "High Temperature Oxidation of UO_2 in Steam-Hydrogen Mixtures," *J. Nucl. Mater.* 208 (1994) 98.

Table 1: Parameters for the Simulation of the X-2 Experiments and Commercial Spent Defective Element Irradiation

Experiment	Model Input							Average O/U Ratio		Fuel Melting	
	Operating History			Fixed Parameters			Adjusted Parameter q_1 (%)	Model ^(a)	Exp. ^(b) (Post-irradiation exam)	Model (Fuel Centreline Temperature (K))	Exp. (Post-irradiation exam)
	Linear Power, P (kW/m)	Post-Defect Residence Time, t (d)	Fuel Surface Temp., T_1 (K)	Porosity, ϵ	σ (m ⁻¹)	Tortuosity, τ					
A. CRL X-2 Exps.											
<i>Artificial Defects</i>											
FDO-687 (Phase I)	64/55	40/40	870/870	0.0237/0.0237	1350/1350	1.023/1.023	0.18/0.18	2.15/2.14	-/-	Yes (2880)/No (2560)	Yes/No
FFO-103	50	15	870	0.0237	1350	1.023	0	2.17	2.28 ^(c)	Yes (2860)	Yes
<i>Natural Defects</i>											
FFO-102-2	67	20	870	0.0237	1350	1.023	0.13	2.16	2.16 ^(d)	Yes (3220)	Yes
FFO-104	58	16	870	0.0237	1350	1.023	43	2.026	2.026 ^(e)	No (2480)	No
B. CANDU Spent Defective Element	~29 (Max.) + ~2	~15 + ~40	800 ~600	0.0237 0.0237	1350 1350	1.023 1.023	0.24 0.24	2.044 2.044	- 2.044 ^(f)	No (1360) No (620)	- No

- (a) The model prediction is based on the stated linear power and corresponds to an average value of the radial stoichiometry deviation profile based on a volumetric-average for a cylindrical pellet (see text).
- (b) The measured O/U ratio represents an average value for approximately a single pellet sample.
- (c) Measured at the mid-length position of element A3N.
- (d) Measured between the secondary and main defect area of element A7E (~40 mm from the bottom end of the fuel element).
- (e) Measured at the mid-length position of element A2F.
- (f) Measured value obtained from cut #4 in Ref. 23.

**Figure 1. Schematic for defective fuel oxidation model.**

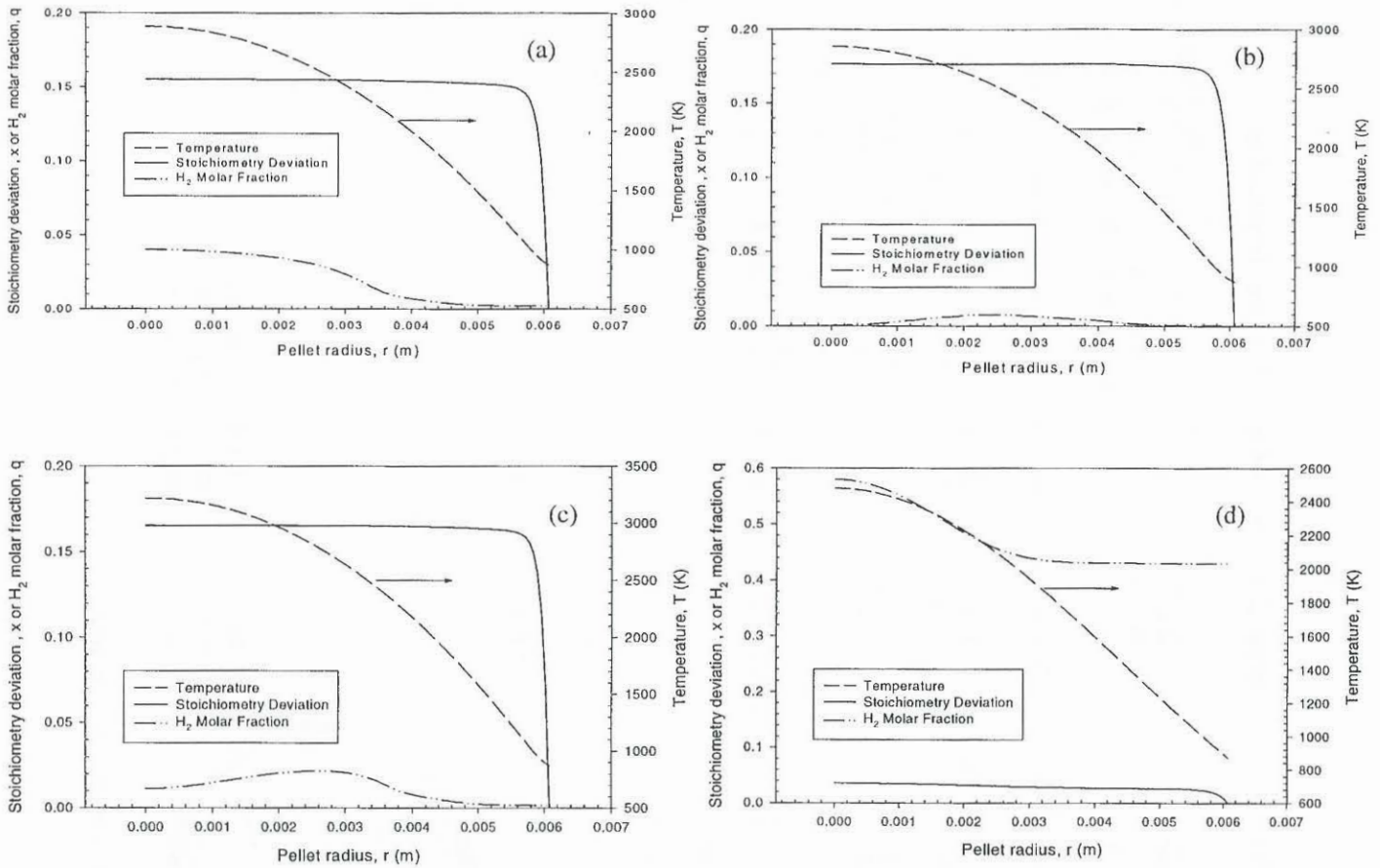


Figure 2. FEMLAB model predictions of the profiles of the hydrogen mole fractions, stoichiometry deviations and fuel temperatures for (a) FDO-687, (b) FFO-103, (c) FFO-102-2 and (d) FFO-104.

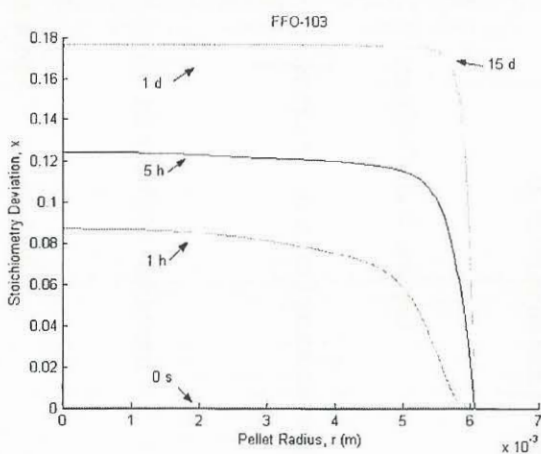


Figure 3. Stoichiometry deviation profiles for FFO-103 as a function of time.

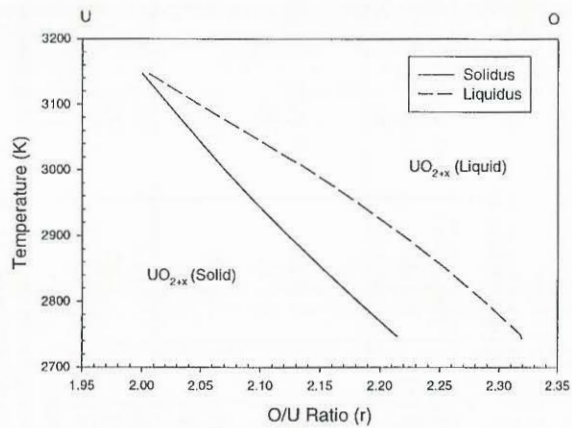


Figure 4. Solidus and liquidus temperatures for the U-O binary phase diagram as predicted by FACT (for the hyperstoichiometry side).

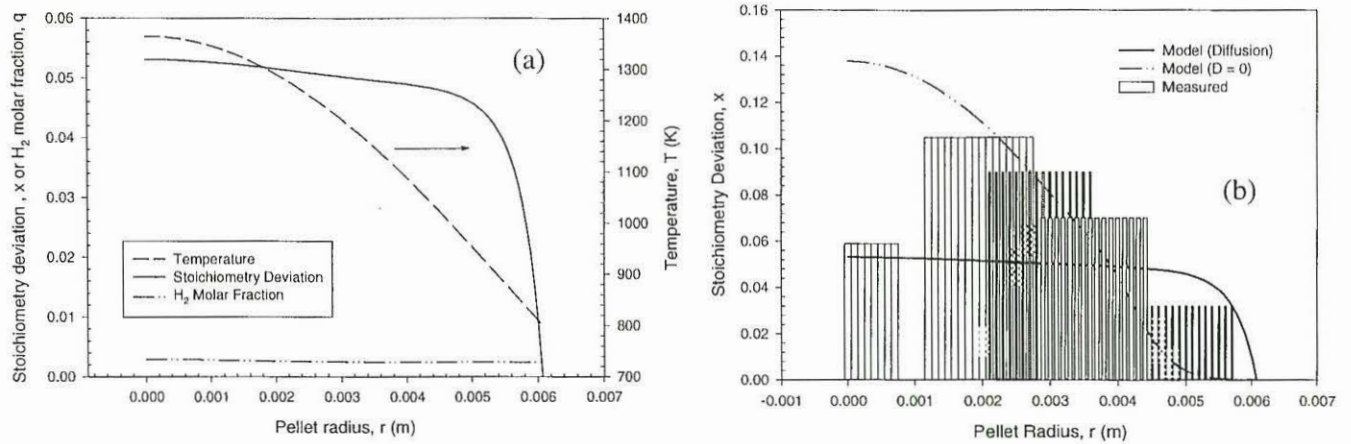


Figure 5. (a) FEMLAB model predictions of the profiles of the hydrogen mole fractions, stoichiometry deviations and fuel temperatures for a spent defective CANDU fuel element. (b) Comparison of measured and model predictions of the stoichiometry deviation profile. The model predictions are shown with solid-state diffusion and without diffusion. All curves yield a pellet-average stoichiometric deviation of 0.044.